minerals

MDPI

Article

Influence of Genetic Processes on Geochemistry of Fe-oxy-Hydroxides in Supergene Zn Non-Sulfide Deposits

Licia Santoro [1,*], Francesco Putzolu [2], Nicola Mondillo [1,2], Maria Boni [1,2] and Richard Herrington [1]

1 Earth Sciences Department, Natural History Museum, Cromwell Road, London SW7 5BD, UK; nicola.mondillo@unina.it (N.M.); boni@unina.it (M.B.); r.herrington@nhm.ac.uk (R.H.)
2 Dipartimento di Scienze della Terra, dell'Ambiente e delle Risorse, Università degli Studi di Napoli Federico II, 80126 Napoli, Italy; francesco.putzolu@unina.it
* Correspondence: licia.santoro85@gmail.com or l.santoro@nhm.ac.uk

Received: 12 June 2020; Accepted: 29 June 2020; Published: 1 July 2020

Abstract: In supergene Zn non-sulfide deposits, the Fe-oxy-hydroxides (FeO/OH) are mainly concentrated in the residual zones (gossan) on top of the oxidized ore bodies, although they can also be found throughout the whole weathering profile coexisting with the primary and secondary ore assemblages. Fe-oxy-hydroxides are rarely pure as they form in systems where a wide range of metals, most of them of economic importance (e.g., Zn, Pb, Co, REE, Sc, Ga, Ge, V, etc.), freely circulate and can be "captured" under specific conditions. Although their occurrence can be widespread, and they have a potential to scavenge and accumulate critical metals, FeO/OH are considered gangue phases during the existing processing routes of Zn non-sulfide ores. Moreover, very little is known about the role of the deposit type on the geochemistry of FeO/OH formed in a specific association. Therefore, this paper provides a comprehensive assessment of the trace element footprint of FeO/OH from a number of Zn non-sulfide deposits, in order to define parameters controlling the metals' enrichment process in the mineral phase. To achieve this, we selected FeO/OH-bearing mineralized samples from four supergene Zn non-sulfide ores in diverse settings, namely Hakkari (Turkey), Jabali (Yemen), Cristal (Peru) and Kabwe (Zambia). The petrography of FeO/OH was investigated by means of scanning electron microscope energy dispersive analysis (SEM-EDS), while the trace element composition was assessed using laser ablation-ICP-MS (LA-ICP-MS). Statistical analyses performed on LA-ICP-MS data defined several interelement associations, which can be ascribed to the different nature of the studied deposits, the dominant ore-formation process and subsequent evolution of the deposits and the environmental conditions under which FeO/OH phases were formed. Based on our results, the main new inferences are: (A) Zinc, Si, Pb, Ga and Ge enrichment in FeO/OH is favored in ores where the direct replacement of sulfides is the dominant process and/or where the pyrite is abundant (e.g., Cristal and Hakkari). (B) When the dissolution of the host-rock is a key process during the supergene ore formation (i.e., Jabali), the buffering toward basic pH of the solutions favors the uptake in FeO/OH of elements leached from the host carbonate rock (i.e., Mn), whilst restricting the uptake of elements derived from the dissolution of sulfides (i.e., Zn, Pb, Ga and Ge), as well as silica. (C) The input of exotic phases can produce significant enrichment in "unconventional" metals in FeO/OH (i.e., Cr and Co at Kabwe; Y at Cristal) depending on whether the optimal pH-Eh conditions are attained. (D) In the Kabwe deposit, FeO/OH records heterogeneous geochemical conditions within the system: where locally basic conditions prevailed during the alteration process, the V and U concentration in FeO/OH is favored; yet conversely, more acidic weathering produced Zn- and Si-bearing FeO/OH.

Keywords: Fe-oxy-hydroxides; LA-ICP-MS; multivariate statistical analysis; trace elements; Zn non-sulfides; gossan

1. Introduction

Non-sulfide Zn-Pb deposits, formerly known as Calamines from the Polish word *"galman"* [1–3], consist of ores formed by the oxidization of primary sulfide bodies. Their most common precursors are Mississippi Valley-type (MVT), Sedimentary Exhalative (SEDEX) and Volcanic Massive Sulfide (VMS) deposits, followed by Carbonate Replacement Deposits (CRD) and sphalerite-rich skarn ores. Depending on their genesis and mineralogical composition, the non-sulfide deposits are commonly classified between hypogene and supergene [1–3]. Hypogene deposits form either by hydrothermal and/or metamorphic fluids altering the chemistry of primary sulfides (e.g., pyrite/marcasite, sphalerite, galena), and resulting in the precipitation of anhydrous Zn silicates and oxides, such as willemite, zincite and franklinite, locally coexisting with sulfides [2]. Supergene deposits derive from the oxidation of primary ores in surficial environments. Under these conditions, the meteoric waters, commonly mixed with groundwaters, react with primary sulfides and leach out the metallic elements (Fe, Zn, Pb, As, etc.), which precipitate as secondary Zn and Pb hydrous silicates and carbonates, such as hemimorphite, sauconite, smithsonite and cerussite, when suitable T, pH and Eh conditions are attained [2]. During this process, large amounts of Fe-oxy-hydroxides (hereafter, FeO/OH) form, consisting of minerals such as goethite, lepidocrocite, maghemite, ferrihydrite and hematite, formed as a result of the breakdown of Fe-rich hypogene mineralogical species (e.g., pyrite, marcasite, pyrrhotite and Fe-rich sphalerite) [4]. In supergene Zn-Pb deposits, FeO/OH are mainly concentrated in the residual zones (gossan) on top of the mineralized oxidation zone, though they can be found throughout the whole weathering profile coexisting with non-sulfide ores. These minerals are rarely pure; on the contrary, they often contain elevated contents of economically significant metals (e.g., Zn, Pb, Co, REEs, Sc, Ga, Ge, In, V), as well as deleterious elements (i.e., Hg, Cd, Cr), and more common cations (i.e., Ca, Mn, Si and Mg). All these elements freely circulate in groundwater and can be adsorbed and/or incorporated in FeO/OH as a consequence of the high specific surface areas of their particles and strong affinities for the surface-binding heavy metals [5–11]. The mechanism accounting for "metallic impurities" incorporation into/onto the FeO/OH is not always straightforward but depends on several parameters in the system precipitating the minerals. In general, the cation substitution of Fe^{3+} within lattice is strictly dependent on the valence of the metal cations (i.e., Ni^{2+}, Zn^{2+}, Al^{3+}, Pb^{2+}, etc.) and the crystal structure of the FeO/OH species (i.e., unit cell parameters such as ionic radius, cell volume, unit cell length, etc., References [8,9] and references therein). The adsorption, which is commonly the precursor for substitution [8], is instead a process that involves interactions between adsorbing species and the surficial hydroxyl groups on the FeO/OH. The adsorption of simple inorganic anion, oxyanions and organic ions on FeO/OH was fully investigated and reported in Reference [8]. The results indicate that the adsorption can occur either by simple replacement of surface hydroxyl groups by an anion (such as silicate, phosphate, chloride, arsenate anions) or via formation of complexes where at least one H_2O molecule is retained by the adsorbing species between the surface and the anion (such as nitrate and perchlorate anions) [8].

Many of the aforementioned metals (i.e., Co, Ga, Ge, Sc, REEs, etc.) are considered "critical elements" [12] and have high economic potential in the modern industry, due to the role they cover in the development of the high-tech devices (e.g., smart phones, electric turbines) and to their supply risk [13]. In rare cases, the weathering of primary orebodies can produce remarkable enrichments of economic metals in FeO/OH and these can represent ore minerals of interest in the supergene section of deposits. An example is the Apex Mine (Utah, USA), where goethite and hematite contain up to ca. 1 wt% Ge and ca. 2 wt% Ga [14,15].

A few research papers on the geochemistry of FeO/OH associated with supergene non-sulfide mineralization have been published by Mondillo et al. [16–20], Santoro et al. [21–23], Navarro-Ciurana et al. [24], Arfè et al. [25,26] and Stavinga et al. [27]. In their studies, they report that the FeO/OH are commonly enriched in Zn and Pb with traces of several other elements, such as As, Cd, Co, Cu, Ga, Ge, Hg, In, Mo, Ni, Sb, Sc and V. This enrichment can depend on: (i) the chemistry of the primary deposit, and (ii) the pH, Eh and T properties of the fluids circulating during the formation of the deposit [28].

However, to date, dedicated studies dealing solely on the trace elements' geochemistry of FeO/OH in Zn non-sulfides are lacking. An accurate knowledge of the geochemistry of FeO/OH associated with the economic supergene non-sulfide Zn-Pb deposits can further help to constrain the parameters driving the precipitation of the secondary mineral assemblages from circulating fluids, and hence highlight the main factors driving the formation of these deposits. The main aim of this study was to evaluate the geochemistry of FeO/OH phases, mainly focusing on goethite and hematite occurring in supergene non-sulfide deposits, with the scope of determining their chemical diversity and assessing the main controlling factors governing the uptake of the metals. An accurate mineralogical and geochemical study was carried out using scanning electron microscope (SEM-EDS) and laser ablation (LA-ICP-MS) on FeO/OH occurring in two different supergene Zn-Pb non-sulfide mining prospects: (i) Hakkari (Turkey) and (ii) Jabali (Yemen). These new data were compared with similar information already published on goethite and hematite from Cristal (Peru) and Kabwe (Zambia) [18,19], using multivariate statistical analysis methods, namely, principal component analysis (PCA), Multivariate Analysis of Variance (MANOVA) and the post hoc Tukey's HSD (Honestly Significant Difference) test, using trace element analytical data. To better discuss the context of the geochemical analyses, we also use unpublished textural and microanalytical data of FeO/OH from the Kabwe deposit [19].

2. Previous Studies on the Considered Deposits

2.1. The Hakkari Prospect (Turkey)

The Hakkari prospect is located approximately 10 km west of the town of the same name in southeastern Turkey. The deposit is located on the northern edge of the Arabian Platform (AP), a few km south of the Bitlis-Zagros suture thrust (Figure 1A) [29]. The ore is hosted within the Cudi Group, consisting of Jurassic shallow-water carbonates overlying Triassic carbonate successions, locally intercalated by mafic lava flows [30,31]. The mineralized area consists of a series of small orebodies (ca. 2.5 Mt each), located in a narrow band of structurally deformed sedimentary rocks [21]. The ore is mainly hosted in a porous and/or brecciated, karstified limestone, locally dolomitized, with interbeds of clastic layers [31,32]. The Hakkari prospect has an estimated resource of 10 Mt at 25% with 40% Zn and 4–8% Pb [33], although potential may amount to several hundreds of millions of tons developed across the >100 km available strike length of the known outcrops [21]. Ceyhan [34] inferred that the primary mineralization consists of an Mississipi Valley Type (MVT) ore formed during the widespread circulation of hydrothermal fluids mobilized by Alpine-Himalayan compressive kinematics. Conversely, Reynolds and Large [35] and Hanilçi [36] considered the Hakkari ores to be a Sedimentary Exhalative (SEDEX)- or an Irish-type deposit, whose genesis can be related to the opening of the Tethys. The hypogene phases are sphalerite, pyrite and galena, accompanied by calcite, dolomite, barite, muscovite and quartz [21,22]. The supergene assemblage, representing the main ore potential, formed during several weathering stages, which are believed to have taken place during Cenozoic, when climate met more favorable conditions, in terms of temperature, humidity and seasonality, for primary deposits to be weathered [21]. During the weathering stages, secondary ore minerals totally or partially replaced the primary assemblages through the precipitation from low-temperature weathering fluids [21,31]. The secondary ore consists mainly of Zn-rich carbonates (smithsonite and hydrozincite) and silicates (hemimorphite), occurring as replacement of the host rock and of the primary ore suite. In this assemblage, Zn-rich FeO/OH phases occur as a porous network of hematite-goethite [21]. Preliminary data from Santoro et al. [22] have shown that in FeO/OH, remarkable amounts of minor to trace elements, such as Zn, Pb and As (up to ca. 10 wt% ZnO, 5 wt% PbO and 2 wt% As_2O_3), occur.

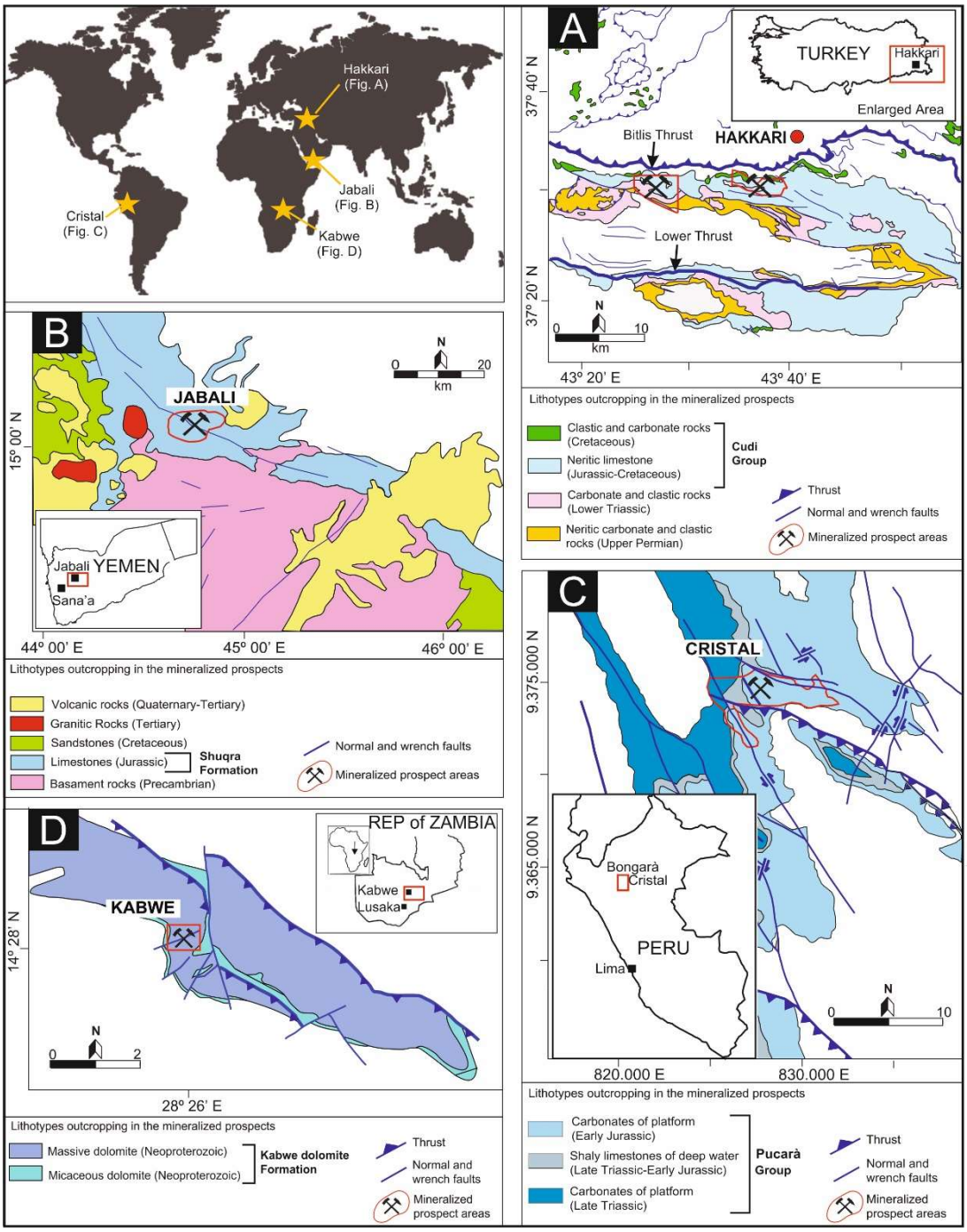

Figure 1. Location and geotectonic framework of the studied deposits: (**A**) Hakkari (Turkey; modified from Reference [29]), (**B**) Jabali (Yemen; modified from Reference [3]), (**C**) Cristal (Peru; modified from Reference [25]), (**D**) Kabwe (Zambia; modified from Reference [2]).

2.2. *The Jabali Deposit (Yemen)*

The Jabali deposit is located 110 km northeast of Sana'a, the capital city of Yemen (Figure 1B) [3]. The ore concentrations are hosted by partly dolomitized marine limestone of the Jurassic Shuqra Formation [16,37,38]. The non-sulfide ore deposit comprises a published resource of 12.6 Mt at 8.9% Zn, 1.2% Pb and 68 ppm Ag. The hypogene mineralization consists of a MVT-like deposit occurring in karst cavities at the top of the Jurassic limestones, hosting sphalerite, galena and pyrite/marcasite as primary ore phases [37,39]. The Rb-Sr dating of the primary ore assemblage provided ages (i.e., 144.0 ± 4.3 Ma)

matching the well-known active rifting and oil generation stages occurring in the area during Late Jurassic–Early Cretaceous [40]. The supergene portion of the deposit forms massive to stratiform bodies located along vertical faults and fractures, comprising smithsonite, with subordinate cerussite, anglesite, sauconite and secondary sulfides. Goethite and hematite are widely spread within the gossan and contain significant amounts of Zn, Pb and Si (up to ca. 12 wt% ZnO, 7 wt% PbO and 6 wt% SiO_2) [16]. Geochemical investigation of stable C-O isotopes of the host rock and Zn-carbonates revealed that the formation of Jabali non-sulfide mineralization is consistent with two main oxidation processes that partially combined: (i) a supergene weathering (early Miocene until recent) and (ii) oxidation related to low-temperature hydrothermal circulation in combination with magmatic-induced geothermal activity in the area (Miocene–Holocene) [16].

2.3. The Cristal Prospect (Peru)

The Cristal prospect is in the Bongará area (northern Peru), 740 km north of Lima. The area lies at the northern extremity of a carbonate belt that extends for 900 km along the eastern flank of the Andean Cordillera, from the Ecuador border to the south. This belt is on the western margin of the Sub Andean Foreland Basin and within the Sub Andean Fold-and-Thrust Belt domain of the Amazonas Region in Peru (Figure 1C) [26]. The Cristal prospect is in the northernmost part of a wider mining district called "Charlotte Bongará Zinc Project" (Zinc One Resources Inc.), which covers an area of approximately 110 km^2. The mineralized area consists of many Zn occurrences that contain mixed sulfide and non-sulfide ores [41,42]. The mineralization is hosted within a Mesozoic (Late Triassic and Early Jurassic) sedimentary succession belonging to the Pucará Group [43], consisting of carbonate rocks ranging from deep-water shaly limestones to platform carbonates, intercalated by silicatic layers. The primary mineralization, considered an MVT-type ore, is hosted in partly dolomitized limestone and consists of Fe- and Ge-bearing sphalerite, with pyrite and rare galena [18,41,42,44–48]. The non-sulfide ore includes mainly hemimorphite and smithsonite, while hydrozincite, chalcophanite, greenockite, sauconite, Zn-bearing mica and synchysite were detected as accessory phases [25,26]. At Cristal, FeO/OH phases are common, either intergrown with the aforementioned secondary assemblage or forming massive layers. Geochemical data from Mondillo et al. [18] (Table S1) have shown that FeO/OH host variable amounts of trace elements. In particular, the goethite from Cristal has high concentrations of Zn, while its Pb grade is significantly lower. Moreover, FeO/OH bear anomalous amounts of Al, Mn, Ni, Ga, Ge, Ti, Co and Y (average ca. 2930, 1640, 15, 5, 180, 28, 18, and 50 ppm, respectively). Recent studies on the stable C and O isotopes of the carbonates in the prospect area confirm that the supergene deposit formed through prolonged weathering of the primary mineralization under humid tropical climatic conditions from Miocene to Recent [26].

2.4. The Kabwe Deposit (Zambia)

The Kabwe deposit (formerly known as Broken Hill) is located in central Zambia, ca. 110 km north of Lusaka (Figure 1D) [2]. The deposit was exploited until 1994 [49] for Zn, Pb, V, Cd, Cu and Ag, which were extracted from the primary sulfide body. Significant Ga and In were also recognized in the primary ores, but never recovered [50]. The mineralization is hosted in the massive dolomite member of the Neoproterozoic Kangomba Formation [49,51,52].

The primary mineralization consists of massive Zn-Pb sulfides, containing sphalerite, galena, pyrite, minor chalcopyrite, accessory briartite and Ge-Cu sulfides, developed in massive dolomite close to the faulted contact with the micaceous dolomite [49,50,53,54]. The genesis of the Kabwe hypogene ore is controversial: several authors have suggested that it consists of MVT-like ore formed from basinal brines during a syntectonic hydrothermal circulation related to the Lufilian orogeny (ca. 550 Ma) [50,55]. Other authors consider Kabwe, together with Kipushi, Dikulushi, Lombe and Kengere deposits, to be a vein-type Zn-Pb-Cu-Ag ore [56]. The non-sulfide resources, estimated at 1.9 Mt, 13.4 wt% Zn, and 1.5 wt% Pb, consist mainly of concentrations of willemite [49,50,54]. Typical supergene minerals, like hemimorphite, cerussite, anglesite, smithsonite, hydrozincite and Fe-oxy-hydroxides,

have overprinted both the sulfide and the willemite mineralization, following different weathering stages likely started in Late Cretaceous–Early Eocene, and lasted until Mio–Pliocene. The climatic conditions and ages are in agreement with the weathering processes which were associated with supergene manganese ores in the Central African Great Lakes region (Democratic Republic of Congo), where the supergene assemblages record weathering stages likely started during relatively cold Late Mesozoic and Paleogene periods (likely Campanian) and ongoing until the more recent humid/warm Neogene [57]. Fe-oxy-hydroxides at Kabwe consist of both goethite and hematite. As shown by Mondillo et al. [19] (Tables S1 and S2), the Zn and Pb amounts in goethite are very erratic (0.50–5.04 wt% PbO and 0.29–5.40 wt% ZnO), while this hydroxide contains significant amounts of Al, Mg, V, Cr, Ni, Ga, Ti and Co (average ca. 1390, 1035, 102, 70, 27, 9, 43 and 38 ppm, respectively). Conversely, hematite is Zn-depleted (average ca. 0.88 wt% ZnO) and shows anomalous concentrations of Al, Mg, U, V and Cr (average ca. 690, 738, 190, 303 and 263 ppm, respectively).

3. Materials and Methods

For this study, the specimens were selected on the basis of previous studies from a wide range of samples from the Natural History Museum in London, UK (NHM) and the Dipartimento di Scienze della Terra, dell'Ambiente e delle Risorse (DiSTAR) at University of Napoli Federico II, (Naples, Italy) collections [16,18,19,21]. New analyses were carried out on 3 FeO/OH-rich specimens (two specimens from Hakkari and one from Jabali; Table 1). Samples H2050 and H2058 were collected from the oxidized horizons at similar depths (6–10 and 4–9 m, respectively) from two different exploration cores of the Hakkari prospect. One specimen (JS Mon 30) was selected from the gossan zone of the Jabali prospect. The samples were selected manually by hand picking but, due to the poor crystallinity of the considered minerals, a complete separation between FeO/OH and the other associated minerals was not always guaranteed. All samples were subjected to X-ray powder diffraction (XRPD), scanning electron microscopy equipped with energy dispersive spectroscopy (SEM-EDS), electron microprobe analyses (EMPA) in wavelengh dispersive spectroscopy (WDS) and laser-ablation ion-coupled plasma mass spectrometry (LA-ICP-MS). Unpublished textural and microanalytical data on FeO/OH from the Kabwe deposit [19] are also included.

Table 1. Specimens used for this study (NHM and DiSTAR ore collections).

Deposit	Specimen ID	Description	Ref.
Jabali	JS Mon 30	Gossan	This study
Hakkari	H2050	Gossan	
	H2058	Gossan	
Kabwe	OR5305	Zinc-silicate ore	Mondillo et al. [19]
	OR5309	Zinc-silicate ore	
	BM.1985,MI29629 2/2	Partly oxidized lead-zinc ore	
	BM.1985,MI29631	Oxidized ore	
	BM1930-372	Partly oxidized sulfide-rich ore	
	BM.1985,MI10900	Hemimorphite and FeO/OH	
Cristal	CR13-1	Gossan	Mondillo et al. [18]
	CR18-19	Hemimorphite and FeO/OH	

XRPD analyses were conducted at the NHM with a Panalytical ExPert Pro MPD automated diffractometer using a CoKα1 radiation operating at 45 kV, 40 mA, with step scan size of 0.02° 2θ. The mineral identification was performed with the HighScore Plus software package. SEM-EDS analyses were carried out using a ZEISS EVO LS 15 scanning electron microscope (NHM) at 20 kV, with 8.5 mm working distance and 3 nA current mounting with X-Max detectors. Quantitative datasets of selected samples were obtained by wavelength dispersion spectrometry (WDS), using a Cameca SX100 electron microprobe operating at 20 kV, 20 nA and 10 μm spot size at the NHM.

The trace elements composition of FeO/OH was determined at the NHM by LA-ICP-MS on an Agilent 7700× quadrupole ICP-MS coupled to a 193 nm ESI NWR ArF excimer laser. The output energy of the laser was typically 3.5 J cm^{-2} and used a 10 Hz pulse repetition rate with a crater size of 35 or 50 µm. Routine measurements of the GSD-1g synthetic basaltic glass (three every 30 unknown analyses) were used as external standards to correct instrumental drift. Dwell times for each element ranged from 5 to 20 ms and peak-hopping was employed. Oxide generation was optimized at ThO+/Th+ = <0.18%. For each analysis, a baseline was measured for 35 s prior to 55 s of ablation. The absolute element concentrations were calculated using ExLAM [58], using the Fe concentration predetermined by SEM-EDS as an internal standard and GSD-1g as the primary reference material. The accuracy of the measurements was monitored by comparing the major element concentrations obtained by LA-ICP-MS with the data obtained by SEM-EDS, as well as repeated analyses of secondary standards (NIST 610, BC 28, Table S3). The analytical procedure used for the samples from the Cristal prospect and the Kabwe deposit are reported in Mondillo et al. [18,19]. The XRPD, SEM-EDS, EPMA and LA-ICP-MS analyses were carried out at the NHM in London by using the same analytical parameters used for the new dataset of Hakkari and Jabali specimens reported above.

Multivariate statistical analysis was conducted on LA-ICP-MS data to compare and contrast FeO/OH from the different deposits studied. Principal component analysis (PCA) was carried out using R software (v 3.6.1), utilizing the packages *princomp* and *ggbiplot*. For the PCA computation, we used 15 variables for a total of 174 LA-ICP-MS point analyses. The relative proportion between variables and observation we used is consistent with the criteria widely used to ensure stable results during PCA computation, i.e., $n > p2 + 3p + 1$, where n is the number of samples and p is the number of variables [59]. The selection of elements used as data input for the statistical analysis has been made based on the variance within the dataset and also considering the importance of a specific element in the mineralized system. Based on the aforementioned criteria, we selected the following elements: Pb, Zn, Si, Ca, Mn, Al, Mg, Cr, V, U, Ge, Ti, Co, Y and Ga. Prior to PCA, the data were normalized using the isometric log ratio transformation, in order to favor the data opening. This transformation requires a matrix of data with no zero. The concentrations below the detection limits (dl) have been represented as a multiplication between the dl and 0.65 [60]. For the interpretation of statistical data, we relied solely on PC with an explained variance ≥10%. Afterwards, to test whether the FeO/OH clusters highlighted by PCA were effectively discriminated by the observed interelement associations, a multivariate analysis of variance (MANOVA test) was also performed. In this case, we have only used the number of PC axes cumulatively explaining at least 95% of the total variance in our samples. In the case of positive results, we then performed a multivariate multiple linear regression between the same PC axes, as dependent variables, and the groups we identified and encoded as dummy independent variables, to feed a post hoc Tukey's test to measure the pairwise differences between groups and to statistically identify which groups cluster together.

4. Results

4.1. Mineralogy, Textures and LA-ICP-MS Geochemistry of the Fe-oxy-Hydroxides

The samples from Hakkari consist of goethite with minor quartz, hemimorphite and cerussite. In agreement with Santoro et al. [21], the BSE imaging of the Hakkari samples confirm that goethite occurs as cryptocrystalline crusts and concretions replacing pyrite (Figure 2A,B). The results of the LA-ICP-MS microanalyses on the selected FeO/OH-bearing specimens of the Hakkari deposit are reported in Table S4 and Figures 3 and 4. In the Hakkari deposit, goethite has a Si content ranging between 1.13 and 3.09 wt%. Lead is commonly present from 3.9 to 8.9 wt%, while the Zn grades range from a minimum of 3.7% to a maximum of 8.1%. All the other trace elements have a concentration systematically below 1 wt%. Calcium (average ca. 1400 ppm), Al (average ca. 590 ppm), Mg (average ca. 220 ppm) and Mn (average ca. 15.2 ppm) yielded the highest values. Although V and Cr occur in traces with low average values (60 and 34 ppm), their concentrations are quite erratic and show broad

variations (9–311 ppm and 4–178 ppm, respectively). Nickel, Ga and Ge are ca. 20 ppm on average, with their peak concentrations never exceeding 50 ppm. Uranium and Ti are ca. 12 and 8 ppm on average respectively, while the average concentrations of Co, Y, La and Ce are ca. <2 ppm.

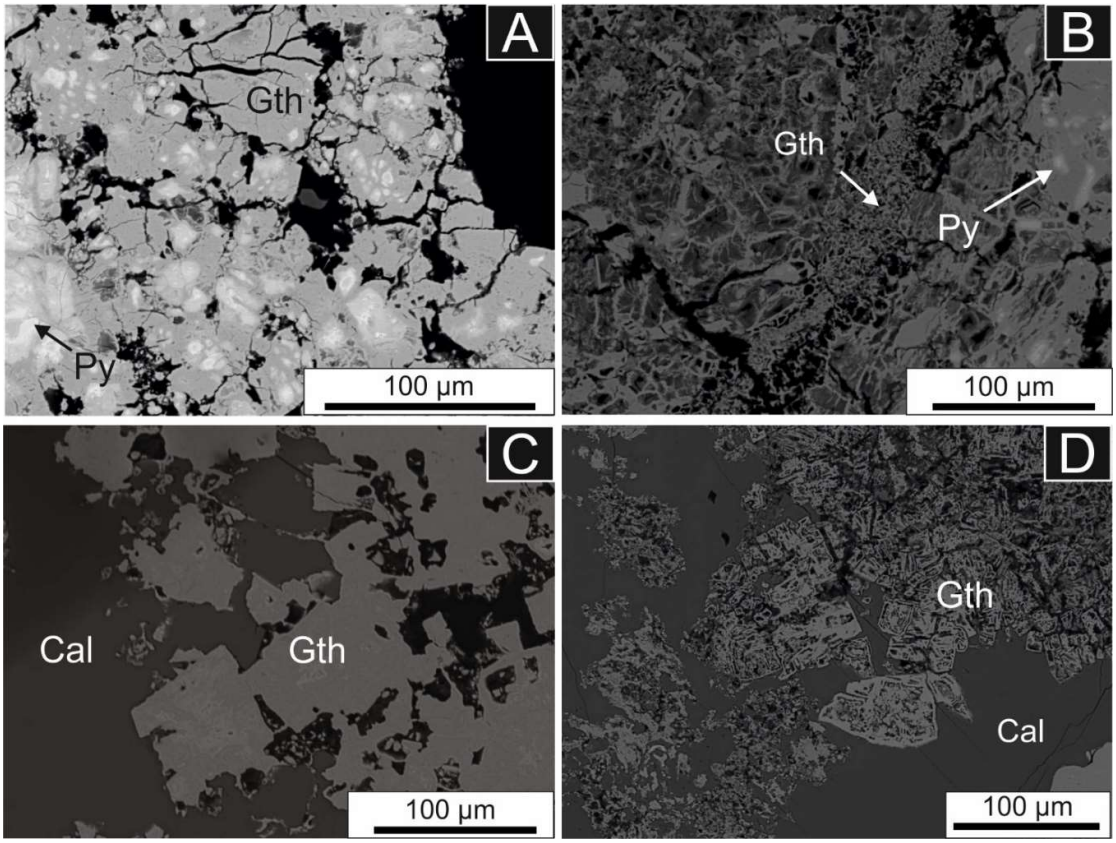

Figure 2. Backscattered Electrons (BSE) images of Fe-oxy-hydroxides occurring in the Jabali and Hakkari deposits: (**A**) and (**B**) cryptocrystalline goethite replacing pyrite (Hakkari), (**C**) goethite pseudomorph after pyrite (Jabali), (**D**) skeletal goethite after pyrite (Jabali). Abbreviations: Gth = goethite, Py = pyrite, Cal = calcite. Abbreviations are from Reference [61].

Goethite from the Jabali specimen occurs as skeletal to massive aggregates after pyrite crystals with minor hematite and calcite (Figure 2B,D). LA-ICP-MS analyses (Table S4; Figures 3 and 4) show amounts of Ca, Al, Mg and Mn in the Jabali FeO/OH higher than those detected at Hakkari: the average Ca content is ca. 1400 ppm, Al instead is slightly higher (average ca. 3500 ppm), while the average concentrations of Mg and Mn are ca. 600 and 1280 ppm, respectively. Vanadium, Cr, Ni, Ge, Ga, U, Ti, Co, Y, La and Ce show lower values compared to FeO/OH from Hakkari: the average concentration of V is ca. 13 ppm, Ni, Ge, Ti and U follow with average values of ca. 8, 9, 7 and 3 ppm, the Cr and Ce grades are ca. 1 ppm, whereas Ga, Co, Y and La are <1 ppm on average. The Si, Pb and Zn contents measured in FeO/OH from Jabali are much lower compared to those of Hakkari. Silicon varies between 0.65 and 0.94 wt%, and the range values of the Pb and Zn grades are 0.06–0.16 wt% and 1.09–2.02 wt%, respectively.

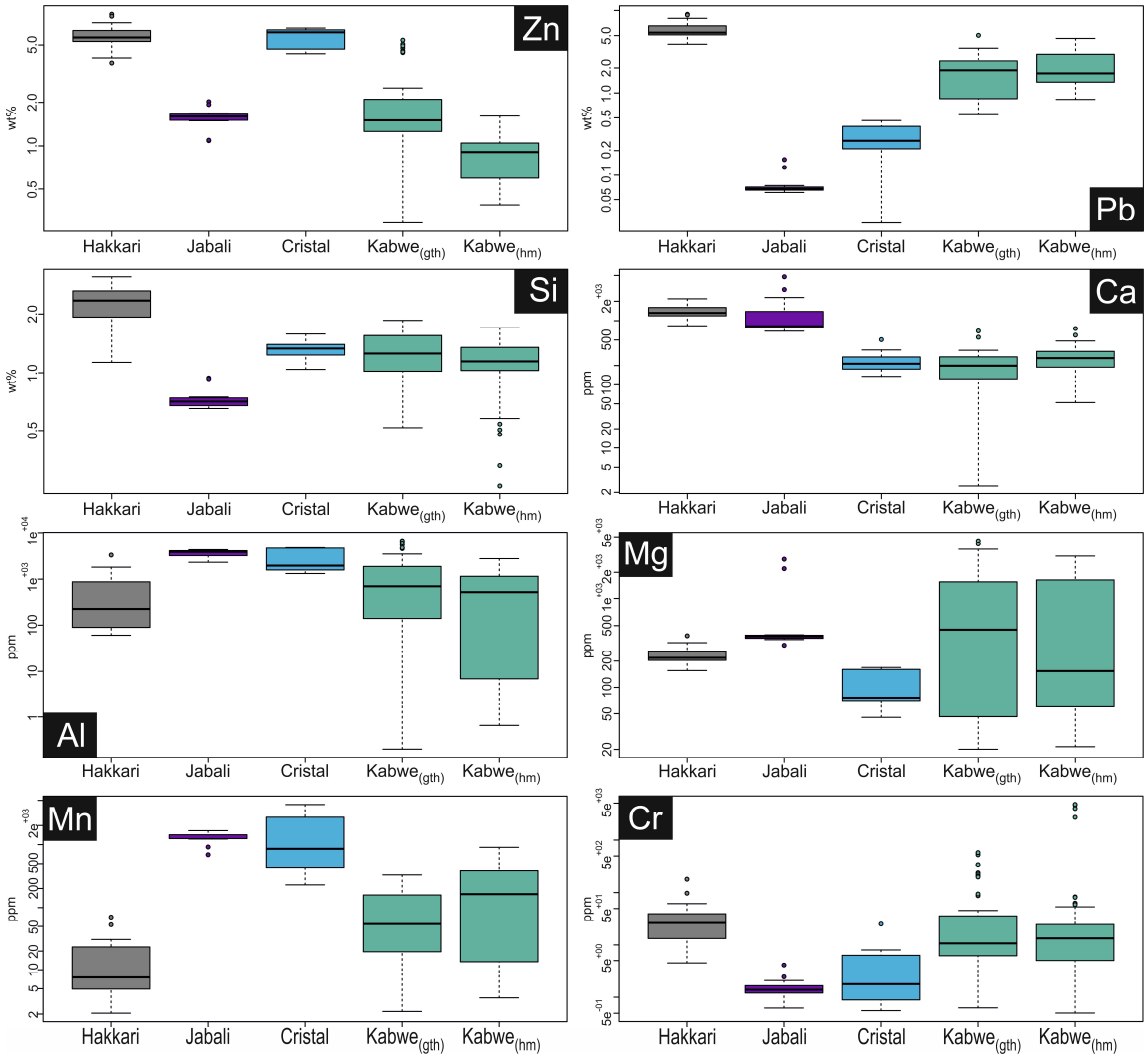

Figure 3. Box and whisker plots showing the chemical composition of the studied FeO/OH from Hakkari and Jabali. Data from Cristal and Kabwe are also reported [18,19].

Fe-oxy-hydroxides in the Cristal deposit consist solely of goethite. As shown by Arfè et al. [26] and Mondillo et al. [18], goethite occurs in the secondary section of the deposit, either in the gossan units, in association with hemimorphite, or in the Zn-carbonate facies, in association with dolomite, Mn-oxy-hydroxides, smithsonite and REE-Fluorocarbonates.

Fe-oxy-hydroxides from the Kabwe deposit, considered for this work, were identified in several samples by Mondillo et al. [19]: BM.1985, MI29629 2/2, BM.1985, MI29631, BM1930-372 and BM.1985, MI10900. For the present work, previous investigations have been reconsidered and interpreted in a new way: on the basis of common textures and mineralogical associations, four distinct FeO/OH types have been distinguished.

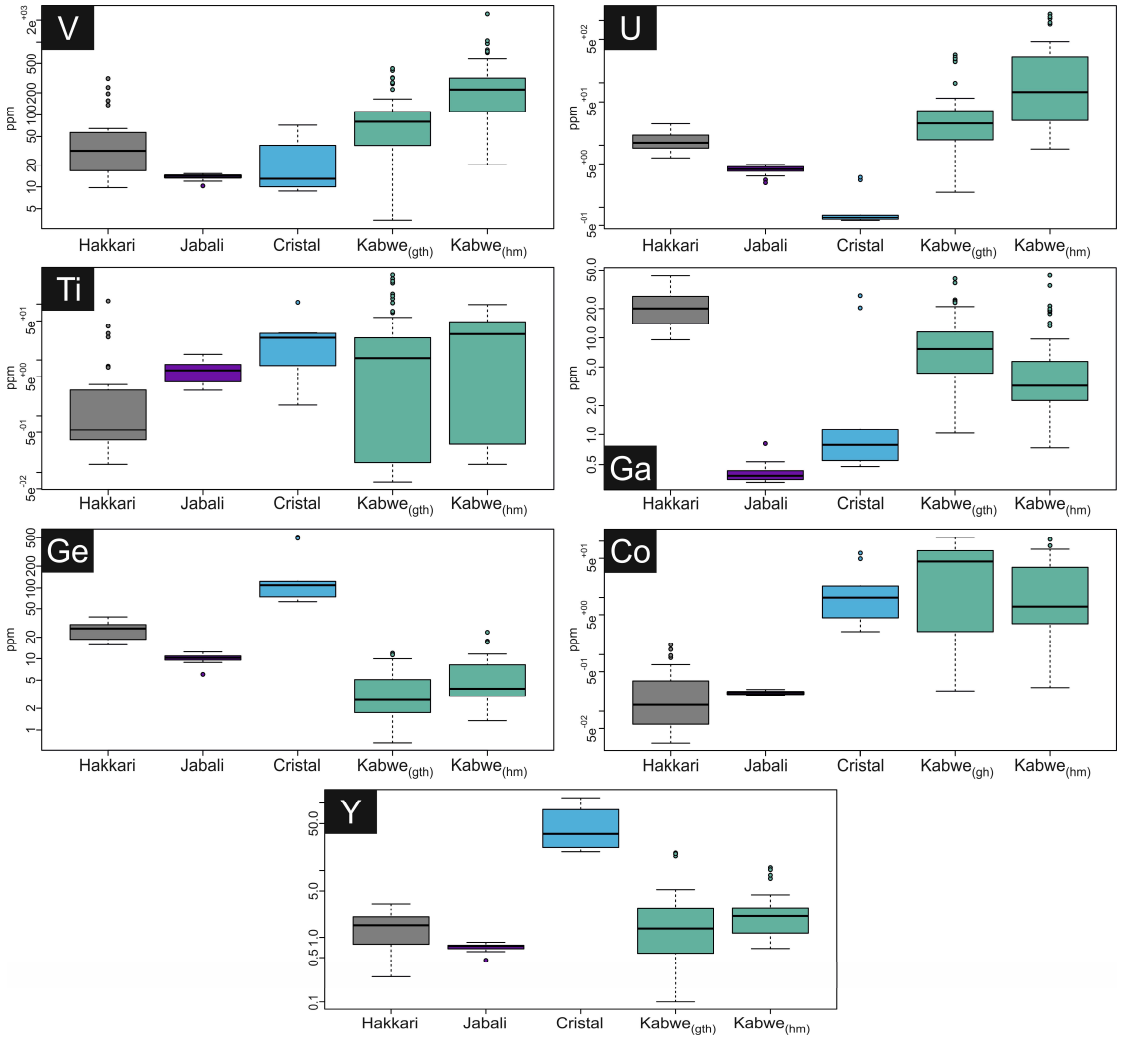

Figure 4. Box and whisker plots showing the chemical composition of the considered FeO/OH from Hakkari and Jabali. Data from Cristal and Kabwe are also reported [18,19].

The Kabwe 1 group consists solely of goethite, occurring in strongly oxidized samples, where Pb-bearing hemimorphite and late-stage Pb-phosphates and Pb(Zn)-vanadates (i.e., pyromorphite and descloizite; Figure 5A) occur as the dominant ore phases (Mondillo et al [19], unpublished data). The Kabwe 2 group consists both of goethite and hematite, which were identified in a sample where sulfides (i.e., sphalerite, galena and pyrite) are directly replaced by willemite and smithsonite. In Kabwe 2, FeO/OH either occur as boxworks or alters pyrite (Figure 5B,C). Hematite and goethite from the Kabwe 3 group form either botryoidal concretions or needle-shaped crystals and occur as late-stage overprints above the non-sulfide assemblage (i.e., descloizite, pyromorphite and willemite; Figure 5D–F). Kabwe 4 goethite and hematite are associated solely with willemite and fluorapatite (Figure 5I–L). FeO/OH also occur as alteration products of willemite (Figure 5G). In addition, FeO/OH are cemented by late-stage phosphates (Figure 5H).

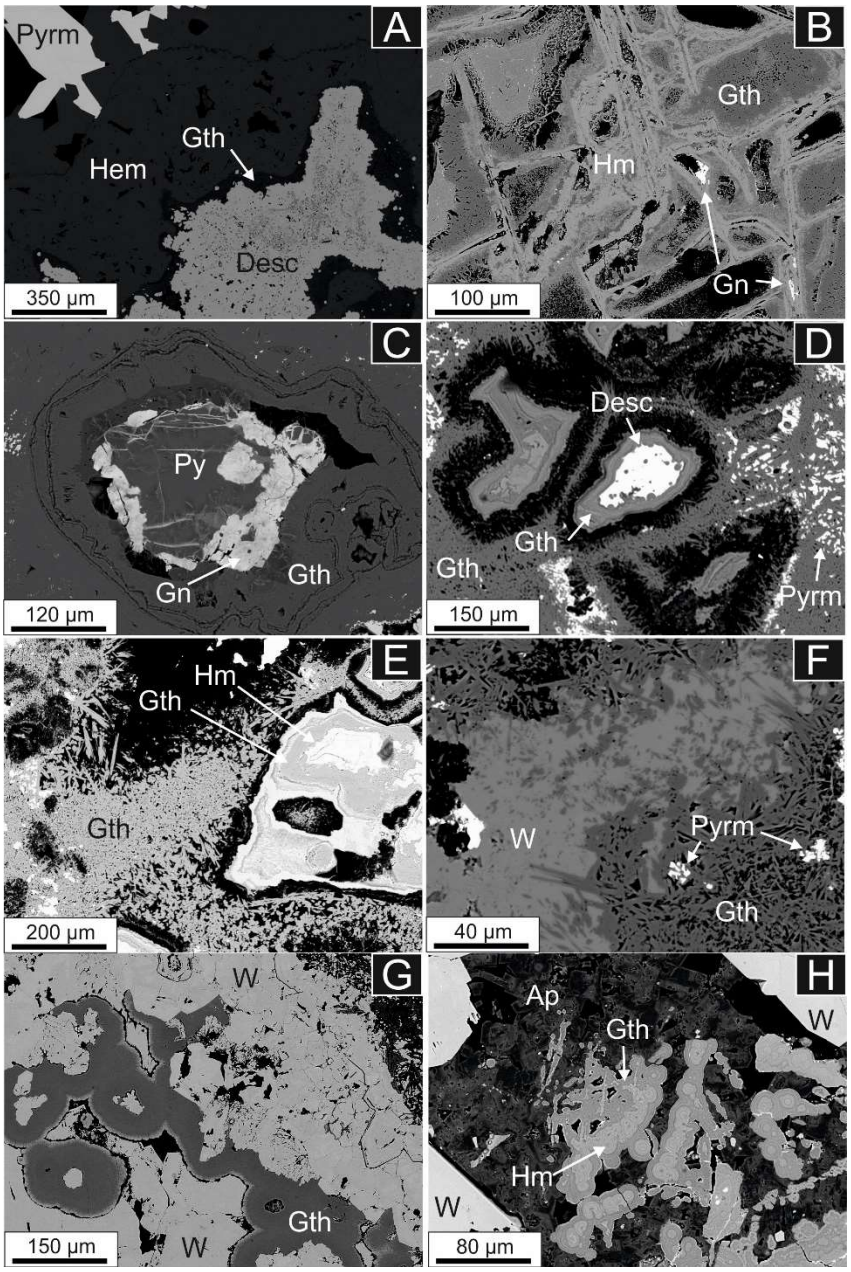

Figure 5. Petrography of Fe-oxy-hydroxides in the Kabwe clusters 1, 2, 3 and 4 (Mondillo et al. [19], unpublished data): (**A**) Cryptocrystalline goethite coating descloizite (Kabwe 1; Sample ID = BM.1985,MI10900), (**B**) Goethite and hematite boxwork with galena relicts (Kabwe 2; Sample ID = BM1930-372), (**C**) Botryoidal goethite replacing pyrite (Kabwe 3; Sample ID = BM.1985,MI29629 2/2), (**D**) Cryptocrystalline-type goethite replacing descloizite and acicular-type goethite intergrowing with pyromorphite (Kabwe 3; Sample ID = OR5305), (**E**) Massive goethite-hematite intergrowth after sulfide (Kabwe 3; Sample ID = OR5305), (**F**) Acicular goethite replacing willemite (Kabwe 3; Sample ID = OR5305), (**G**) Cryptocrystalline goethite replacing willemite (Kabwe 4; Sample ID = OR5309), (**H**) Reworked hematite and goethite cemented by fluorapatite (Kabwe 4; Sample ID = BM.1985,MI29631). Abbreviations: Gth = goethite, Ht = hematite, Desc = descloizite, Hem = hemimorphite, Pyrm = pyromorphite, W = willemite, Sp = sphalerite, Sm = smithsonite, Gn = galena, Ap = fluorapatite. Abbreviations are from Reference [61].

4.2. Multivariate Statistical Analysis

Principal component analysis, carried out on data of FeO/OH from Hakkari, Jabali, Cristal and Kabwe (Figure 6A and Table S5), shows that the first four components (i.e., form PC1 to PC4) exceeded the 10% cut-off value of variance and collectively account for 72.22% of the total explained variance in the dataset. The bi-plot of Figure 6B shows the relationships between the first and second components (PC1 and PC2, respectively).

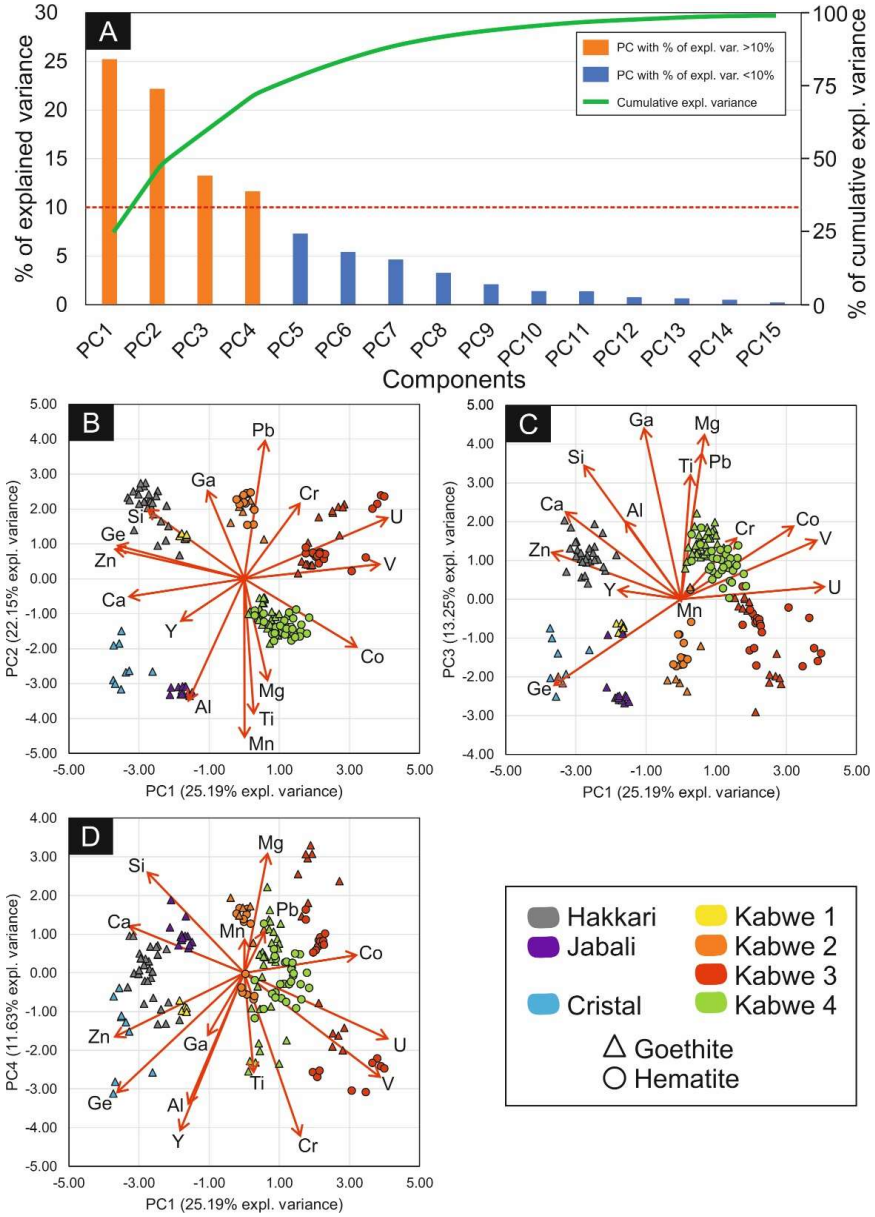

Figure 6. Results of the principal component analysis (PCA): (**A**) Scree plot showing the % of explained variance of each PC of the dataset: (**B**), (**C**) and (**D**) PC1 versus PC_n biplots. Kabwe 1 = sample BM.1985, MI10900; Kabwe 2 = M1930; Kabwe 3 = OR5305 and BM.1985, MI29629 2/2; Kabwe 4 = BM.1985, MI29631 and OR5309.

A relevant aspect observable in the PC1 versus PC2 plot is that overall, samples from different deposits fall within different regions of the diagram and are also characterized by peculiar interelement associations. The PC1 (25.19% explained variance) accounts for a significant decoupling between the Y–Ca–Zn–Ge–Si–(Ga–Al) and the U–V–Co–(Cr) eigenvectors, which along the PC1, have negative

and positive loadings, respectively. The PC2 (22.15% explained variance) controls the geochemical decoupling between Pb–(Ga–Cr) and Mn–Ti–Mg–(Al), whose eigenvectors are showing positive and negative values along the PC2 axis, respectively. In the PC1 versus PC2 plot, goethite samples from the Hakkari deposit are spread within the fourth quadrant as a consequence of the clustering effect of the Zn–Ge–Si–(Ga) group, while goethites from Jabali occur in the third quadrant and are highly correlated with the Al eigenvector. Goethite samples from the Cristal deposit, though occurring in the same region of the Jabali analyses, show a higher association with Y and less with Ca. As regards to FeO/OH from Kabwe (i.e., goethite and hematite), the PCA has shown a more complex statistical distribution. In particular, the analyses from the Kabwe 1 plot in the third quadrant, are close to the goethites from the Hakkari deposit. Each remaining cluster of FeO/OH from Kabwe (i.e., Kabwe 2 to Kabwe 4) comprehends analyses of both goethite and hematite. FeO/OH from Kabwe 2, occurring at the boundary between the fourth and first quadrants, have PC1 scores close to zero, while they show positive PC2 score values. Analyses from Kabwe 2 show a high correlation with Pb, and less with Ga and Cr. Analyses from the Kabwe 3 cluster, having positive PC1 and PC2 score values that fall within the first quadrant, are correlated with U and V, and less so with Cr eigenvectors.

Analyses from Kabwe 1, Kabwe 2 and Kabwe 3 have relatively similar PC2 score values and are only differentiated by the clustering effect provided by the U–V–(Cr) and Ca–Zn–Ge–Si–(Ga) antagonism dominating the PC1.

Another relevant aspect regards the Kabwe 2 and 4 groups, which are characterized by very similar PC1 values (close to zero to slightly positive), although they are found in different regions due to the opposite clustering effect of the Mn–Mg–Pb versus Ti–Cr–(U–V) along the PC2. The Kabwe 4 group falls in the second cluster and has negative PC1 scores and positive PC2 values. This cluster shows a strong relationship with the Co, Ti, Mn and Mg eigenvectors. The PC3 (11.63% explained variance; Figure 6C) accounts for a strong decoupling between the Ge eigenvector, occurring in the third quadrant, and the remaining variables that fall in the upper region of the plot, characterized by positive PC3 score values. Analyses from Cristal, Jabali and Kabwe 1 were revealed to be the most influenced by the clustering effect of the distribution of the Ge variance along the PC3. Another interesting aspect regards the analyses of the Hakkari goethite that, despite being characterized by a significant correlation with Ge on the PC1 axis (Figure 6B), are affected by a decoupling from the Ge in the PC3, following the clustering effect of Zn in the fourth quadrant.

The PC4 (11.63% explained variance; Figure 6D) provides further insights on the geochemical diversity of FeO/OH from the Kabwe clusters 2, 3 and 4, which show negative to positive PC3 score values according to the clustering effect of the opposite Mn–Mg–Pb and Ti–Cr–(U–V) groups. A peculiar aspect of the PC4 is that it produces a clustering that is not in agreement to those outlined by PC1 and PC2, thus producing a de-clustering within the Kabwe groups.

The outcomes of the MANOVA test carried out on the PC1 to PC9 components (cumulative variance ca. 95%; Figure 6A and Table S5) confirmed the existence of statistically significant differences between most of the FeO/OH sample groups showing clustering on the PC1 versus PC2 plot (Pillai = 5.1229, Approximate F = 106.43, p-value < 0.001). The post hoc Tukey's test of the linear combinations of the PC1 to PC9 axes allows to recognize that the groups Hakkari, Jabali, Cristal, Kabwe 1 and Kabwe 3 are statistically diverse (Table 2), whereas the Kabwe 2 and 4 groups do not show significant statistical geochemical differences with the post hoc Tukey's test.

Table 2. Results of the post hoc Tukey's HSD test.

Deposit	Kabwe 3	Hakkari	Kabwe 4	Kabwe 2	Jabali	Kabwe 1	Cristal
Group	a	b	c	c	d	e	f

5. Discussion

5.1. Linking the Element Deportment in Fe-oxy-Hydroxides to the Mineralization Style: Intrinsic Properties of the System Versus Environmental Conditions

Fe-oxy-hydroxides are among the most stable phases in supergene systems, thus their occurrence in the gossan sections, as well as throughout the weathering profiles in secondary Zn-Pb ores, is not unexpected. The coexistence of goethite and hematite in weathered terranes is commonly ascribed to their similar thermodynamic stability, though their proportions in the system are strongly controlled by the ferrihydrite transformation through pH and temperature variations [62,63]. As a general rule, ferrihydrite transformation to hematite is favored at higher temperatures (subtropical and tropical) and neutral pH, whereas goethite is favored at lower temperatures and both high and low pH [64–68]. In the current study, we observed that goethite is ubiquitous in all selected deposits, while significant amounts of hematite were detected solely in the Kabwe deposit [19]. Previous studies have shown that hematite is absent from both the Hakkari and Cristal deposits [18,21,26], while hematite is very minor at Jabali [16].

The LA-ICP-MS data of FeO/OH show a range of contrasting features in terms of minor and trace elements' composition between the selected Zn non-sulfide deposits (Table 3). Based on our results, the FeO/OH can be subdivided in two macro-groups:

(A) FeO/OH, characterized by high concentrations of elements, such as Zn, Pb, Ca, Mn, Mg and Si, that are commonly found in Zn non-sulfide ores.

(B) FeO/OH showing high concentrations of elements, such as Cr, V, U, Y, Ge and Ga, that occur in Zn non-sulfides only under unusual conditions (e.g., nature of the primary ore, exotic input of material, alteration history, etc.).

Table 3. Summary of features and findings on the mineral chemistry of Fe-oxy-hydroxides in the studied deposits. The dominant phases in the mineralogical assemblages are reported in bold.

	Hakkari	Jabali	Cristal	Kabwe
Hypogene mineralogy	**Sphalerite, pyrite**, galena and barite	sphalerite, galena, pyrite/marcasite	**Sphalerite, galena**, pyrite	**Sphalerite, galena, chalcopyrite, willemite**, pyrite, Ge-sulfides
Supergene mineralogy	**Hemimorphite, FeO/OH**, Zn-carbonates, Zn-clays	**Smithsonite**, hydrozincite, hemimorphite, greenockite, FeO/OH	**Hemimorphite, smithsonite**, FeO/OH, Zn-clays	**Willemite, Zn-Pb-vanadates**, smithsonite, phosphates, FeO/OH
Geochemical signature of FeO/OH	Zn-Pb-Si-Ca-Ga	Mn-Mg	Zn-Ge-Y	Zn-Si-(Pb-Ga) and U- V-(Cr-Co)
Enrichment mechanism	Acidity-driven process (direct replacement of sulfides)	Wall-rock replacement process	Acidity-driven process (direct replacement of sulfides)	Local acidity-driven process, superimposed by alkaline process caused by the evolution under arid climate

The different statistical signatures we observed can be discussed in light of the diverse intrinsic properties of the systems (e.g., nature of the primary ore, ore-formation process, alteration history, etc.) and additionally considering the environmental conditions at the time of deposit formation (e.g., pH, Eh, climate regime, etc.).

5.1.1. Hakkari Deposit

Goethites in the Hakkari deposit represent ubiquitous alteration products and are concentrated in the gossan section of the weathering profile [21]. The PCA shows a significant correlation between the data of Hakkari and the eigenvectors of Zn, Pb and Si (Figure 6B; up to 8.10 wt% Zn, 8.98 wt% Pb and 3.09 wt% Si). Furthermore, FeO/OH from this deposit are also characterized by low Mn (Figure 3; up to ca. 70 ppm Mn) and by an enrichment in Ga and Ca (Figures 3 and 4, respectively; up to ca 45 ppm Ga and ca. 2200 ppm Ca) as compared to the other deposits. This signature of goethite from Hakkari is likely due to both the inherited geochemical characteristics of the hypogene mineralization, and to the evolution of the environmental conditions (i.e., pH and Eh). Although Ga can be concentrated in a

range of hydrothermal ores, as volcanic massive sulfide (VMS) deposits, MVT and SEDEX, this element is particularly enriched in primary sulfides (i.e., sphalerite) in low-temperature systems where the role of magmatic fluids in supplying the metals is commonly negligible [69]. In the Hakkari deposit, though the nature of the primary mineralization is still in doubt, the occurrence of the As–Sb–Tl (≫Hg) geochemical association points to a primary ore significantly different from a typical MVT, and more resembles a SEDEX- or CRD-type setting [21,36]. Therefore, the presence of relatively high Ga concentrations in goethite, rather than being explained by its abundance in the primary ore, can be ascribed to the existence of the optimal environmental conditions for its uptake in FeO/OH during the weathering stage. In surficial settings, at ambient temperature of ca. 25 °C, Ga is immobile in a wide range of pH, i.e., from 3 to 8 [28]. The Ga enrichment in FeO/OH is a common process during chemical weathering and has been observed to occur commonly during the ore-formation process of bauxite and laterite ores [70], where the Ga incorporation in FeO/OH, rather than in Al-hydroxides, occurs when the pH of the metal-bearing solution is very low (pH < 4). The prevailing acidity during the formation of the Hakkari non-sulfide ore might have also controlled the abundance of FeO/OH, as well as the development of extensive gossan sections within the weathering profile. In fact, the high amount of sulfuric acid produced from the alteration of pyrite-bearing massive sulfide assemblage might have resulted in the override of the buffering effect of the wall-rock, leading to the formation of a non-sulfide assemblage under acidic conditions [2]. Under these conditions, the prevailing acidity of the system might have also increased the capability of goethite to concentrate Pb, Zn, Si and Ca, while preventing Mn uptake. More specifically, Lu et al. [71] have proposed that the co-precipitation of Pb^{2+} in goethite is very significant under acidic conditions (ca. pH 4). Furthermore, other studies [72,73] have described that the goethite has an increased potential in scavenging a range of bivalent metals, among which are Zn^{2+} and Pb^{2+}, in the presence of SO_4^{2-} anions, with the latter favoring the formation of Pb- and Zn-SO_4 ternary complexes at the goethite–water interface. As regards Si, we observed that goethite from Hakkari is particularly Si-rich in comparison with the other deposits. Even though Si is systematically found as a trace element in FeO/OH occurring in Zn non-sulfide ores, its mechanism of speciation has not been confirmed. The availability of Si during the ore formation process, either from the occurrence of siliciclastic layers or cherty limestones within the sedimentary sequence, is a key aspect in defining the nature of the secondary ore assemblage, as it enhances the formation of Zn-silicate ores (i.e., hemimorphite and/or sauconite) [74]. At Hakkari, the sole Zn-silicate found in the ore is hemimorphite, which in a few localized areas is more abundant than Zn-carbonates [21]. Precipitation of hemimorphite is controlled by the pH of the system (i.e., it is stable at pH < 7), it forms when sufficient H_2SO_4 is generated by sulfide weathering, and precipitation is also enhanced by an increased Si activity and thus by the amount of Si dissolved from the wall-rock [2,75]. In addition, the pH of the system and Si availability appear to have controlled the chemistry of goethite occurring in the gossan. The limited values of Mn in goethite at Hakkari, as compared with the other deposits, may reflect the paucity of this element in the Hakkari system itself. In Zn non-sulfide deposits, Mn comes from the dissolution of Mn-bearing carbonates [76]. In this context, the Hakkari ore is characterized by hydrothermal carbonates (i.e., calcite and dolomite) that show uncharacteristically low Mn concentrations [21]. However, Santoro et al. [21] have shown that Mn can locally reach significant values in a few localities of the prospect, where chalcophanite-like phases were found, meaning that the lack of Mn in goethite was also likely to have been controlled by the physico-chemical conditions in the gossan. In the Hakkari gossan, like in lateritic ores developed in regoliths, the elevated acidity may have enhanced the Mn leaching process and its dispersion into other ore zones, where more neutral to basic pH caused its precipitation as Mn-oxy-hydroxides [77]. Significant amounts of Ca in goethite could be related to the nature of the host rock, which in the Hakkari deposit consists mainly of limestone [21], more susceptible to karstification than dolomite, and thus might have caused an increase of the available amount of Ca during FeO/OH formation.

5.1.2. Jabali Deposit

In the Jabali deposit, FeO/OH is largely goethite and is mostly concentrated in the gossan, although it also occurs as a minor phase within the dedolomitized zones of the host-rock [16]. The PCA on LA-ICP-MS data (Figure 6B) has shown that the eigenvectors of Mn and Al, and less so that of Mg, exert the most significant clustering effect along the PC2 on the Jabali data. This also accounted for the significant decoupling of the Jabali data from the eigenvectors of Pb, Zn, Ga and Si, reflecting the general depletion of these elements in FeO/OH from the Jabali ore (Figures 3 and 4). The presence of high concentrations of Mn in goethite from Jabali (up to ca. 1700 ppm Mn) points to a contrasting Mn behavior compared to Hakkari, where this element has been leached from the gossan zone. The more effective trapping of Mn in the Jabali system may be linked to the peculiar alteration history experienced by the host carbonates. As shown by Mondillo et al. [16], the hydrothermal $Fe^{2+}(Mn^{2+})$-bearing dolomite in the wall-rock underwent an intense oxidative-driven dedolomitization process due to the oxidation of Fe and Mn, which ended with the formation of calcite and Fe^{3+}- and Mn^{4+}-oxy-hydroxides [16]. Moreover, during this dedolomitization, the precipitation of Mn- and Fe-oxy-hydroxides was also accompanied by the release of Mg^{2+} in solution, which would also explain the outliers of Mg data observed in the Jabali goethite (Figure 3). The significant association observed between the Jabali data and the Al eigenvector is likely related to two key aspects: (i) except for Mn, the goethite from Jabali is characterized either by very low trace elements' concentrations (i.e., Pb, Zn, Si, Cr, Ga and V), or by trace elements' amounts in the range of the baseline of the other deposits (i.e., Ca, Y, Ge, Co and U). (ii) Even though the Al amounts are very high in the goethite from Jabali (up to ca. 4300 ppm Al), this metal is widespread in all the analyzed FeO/OH. Therefore, the depletion of Pb, Zn, Si and Ga in goethite (up to 0.16 wt% Pb, 2.02 wt% Zn, 0.94 wt% Si and ca. 1 ppm Ga) resulted in poor correlation between these elements and the goethites, and better correlation with Al (Figure 6B). This is probably linked to the formation processes acting during the precipitation of the non-sulfide assemblages in terms of pH. As shown by Mondillo et al. [16], the Jabali non-sulfide body is dominated by an extensive wall-rock replacement process. This means that Zn-bearing acid solutions reacted and were buffered by significant portions of the host dolomite. This neutral to slightly basic pH played a key role in defining the Zn-, Pb-, Si- and Ga-depleted geochemistry of the FeO/OH, being those elements commonly concentrated in FeO/OH formed in acid environments.

5.1.3. Cristal Deposit

The PCA analysis has shown that most of the variance of Ge and Y in the dataset (up to ca. 510 ppm Ge and 120 ppm Y) is explained by the data distribution of the Cristal analyses in the PC1 versus PC2 and PC1 versus PC3 projections (Figure 6B,C, respectively).

In the PC1 versus PC4 projection (Figure 6C), the Zn eigenvector also exerts a minor clustering effect on goethites from Cristal, which is due to their high Zn contents (up to ca. 6.50 wt% Zn), similar to those observed in the FeO/OH from Hakkari (Figure 3). Although goethite from Cristal also has significant amounts of Si and of minor Pb (Figure 3; up to 1.58 wt% Si and 0.46 wt% Pb), the absence of clustering between the aforementioned elements and the data from Cristal is likely to be due to the masking effect of data from other deposits (Hakkari and Kabwe) that have higher contents of those elements. As discussed by Mondillo et al. [18], the high Ge amount occurring in the secondary phases can be related to: (i) anomalous Ge enrichments in primary sphalerite and (ii) favorable geochemical conditions governing the supergene processes, which led to a conservative behavior of Ge, limiting its leaching from the system. Regarding point (ii), Mondillo et al. [18] inferred that the acidity-driven (pH < 7) oxidation process led to the formation of Ge-bearing hemimorphite within the siliciclastic horizons of the ore, and to the Ge-endowed goethite in the gossan layers. The formation and evolution under acid conditions might have also enhanced the concentration process of Zn, Pb and Si in goethite by following the same patterns mentioned for Hakkari (see Section 5.1.1). Experimental studies [78] conducted on the capability of FeO/OH in scavenging lanthanides have shown that at pH < 6, the adsorption of heavy REEs overcomes that of light REEs (La to Nd), with the exception of

Ce giving rise to positive anomalies. Assuming that Y has a similar geochemical behavior of heavy REE (i.e., Dy to Lu; HREE), it is likely that the incorporation of REE + Y in the Cristal goethite was also pH-controlled and favored by the presence of low pH environments during FeO/OH formation.

5.1.4. Kabwe Deposit

Fe-oxy-hydroxides (i.e., goethite and hematite) in the Kabwe deposit can be classified into four groups (i.e., Kabwe 1 to 4) that have distinct textures, parageneses, chemistry (Figures S1–S3) and diverse interelement associations. The first principal component of the PCA (Figure 6B), allows us to distinguish two significantly contrasting associations of elements among the data: Zn–Si–(Pb-Ga) and the U–V–(Cr), which correspond to the Kabwe 1 and Kabwe 3 group "end-members". The Kabwe 2 group, having a strong relationship with Pb and a relatively poor correlation with Ga and Cr, shows an intermediate distribution between the previous two groups. The Kabwe 4 group, despite showing a stronger relationship with Co along the PC2 and with Ti along the PC3 (Figure 6B,C), has the same PC1 scores as Kabwe 2. This similarity has also been confirmed by the Tukey's test (Table 2), which shows no significant statistical difference between the Kabwe 2 and 3 groups. Regarding goethites from the Kabwe 1 group, their high Si and Zn grades (up to 1.80 wt% Si, 5.40 wt% Zn), as well as the association of FeO/OH with hemimorphite, are very similar to those of the Hakkari ore. These observations suggest that FeO/OH formed during acid conditions during the ore-formation process (see Section 5.1.1). The local acidity-driven processes are also supported by the occurrence of descloizite in close association with FeO/OH (Figure 5A) since Boni et al. [79] demonstrated that the precipitation of Pb-vanadates requires acidic conditions, sourced from the oxidation of sulfides. The main peculiarity of FeO/OH of the Kabwe 2 group is their close association with Pb and Ga (up to 5.04 wt% Pb and 44 ppm Ga). Even though these are distinctive characteristics, they cannot be directly linked to a difference in the environmental conditions if compared to Kabwe 1, by considering solely the differences between the Pb-Ga and Zn-Si pairs. The most significant geochemical difference between Kabwe 1 and 2 is actually found when comparing Ga versus Ge contents. In both groups, Ge is very low (4–7 ppm Ge in Kabwe 1 and 8–11 ppm Ge in Kabwe 2), while the Ga concentration is significant in Kabwe 2 (14–44 ppm Ga), and low in Kabwe 1 (4–5 ppm Ga). According to Wood and Samson [28], at slightly neutral pH, Ga is more immobile than Ge, which means that the displacement of the Kabwe 2 point analyses toward higher values of the PC1, due to higher Pb and Ga grades, might record less acidic conditions occurring locally within the oxidized section of the ore. This is also supported by the occurrence of minor smithsonite in Kabwe 2 samples [18], which forms under neutral to basic pHs [2]. As regards the high Pb amounts in FeO/OH from Kabwe 2, the most reliable explanation can be found in the intrinsic mineralogy of the samples, which are particularly rich in galena. The Kabwe 3 FeO/OH group, that is statistically anticorrelated to Kabwe 1, shows the highest PC1 scores and samples show a strong association with V-U-(Cr). A relevant aspect to consider is that FeO/OH occur as replacement of Pb-vanadates, Pb-phosphates and willemite (Figure 5D–F), suggesting that the formation of FeO/OH in this sample occurred outside the optimal condition of stability at pH > 7. Therefore, in the original facies of the Kabwe ore where the Kabwe 3 samples were collected, the formation conditions were likely dramatically different from the acid environment demonstrated in the oxidized facies of the Kabwe 1 sample. This likely resulted in the significant different speciation of trace elements in FeO/OH of the Kabwe 3 group, which are relatively depleted in Zn-Si-(Ga) (up to 2.51 wt% Zn, 1.67 wt% Si and 5 ppm Ga) and enriched in V-U-(Cr) (up to ca. 1000 ppm V, 1200 ppm U and 4700 ppm Cr). This distribution is consistent with the experimental studies of Peacock and Sherman [80] and Sherman et al. [81], which demonstrated that the speciation of V and U in soil systems can be enhanced under neutral to alkaline conditions. Considering that V is transported into solution as calcium metavanadate [$Ca(V^{5+}O_3)_2$], while the mobility of U is constrained to the formation of dicarbonate $U^{6+}O_2(CO_3)_2{\cdot}2H_2O^{2-}$ or tricarbonate $UO_2(CO_3)_3{}^{4-}$ complexes, e.g., Reference [82], it is possible that, similarly to the V-rich non-sulfide ores of the Otavi Mountainland (Namibia), the neutralization of surficial solutions required for remobilization of V and

U might was likely produced by the environmental transition from tropical to arid climatic conditions, e.g., Reference [79]. However, it is also important to consider that, in low T systems, V fixation in FeO/OH is related to V reduction to the trivalent state (V^{3+}) [80]. In the Kabwe deposit, the low $\delta^{13}C$ $‰_{V\text{-}PDB}$ of supergene carbonates suggests a significant input of biogenic C [19], which likely enhanced the formation of local low Eh conditions and also allowed the reduction of V to V^{3+} and its up-taking in FeO/OH. Significant Cr concentrations and trace amounts of Co were also observed in some Kabwe FeO/OH samples (up to ca. 4700 ppm Cr and up to ca. 85 ppm in Kabwe 3; up to 530 ppm Cr and up to 120 ppm Co in Kabwe 4). The Cr and Co uptake in FeO/OH is a widely recognized process in terranes where mafic to ultramafic rocks undergo tropical weathering (e.g., Ni-Co laterites; [83]). However, Cr and Co, as well as V, are not conventional metals occurring in primary sulfide and non-sulfide Zn deposits. Even though the enrichment in Co at Kabwe can be most probably related to the presence of one of the largest Cu-Co deposits on earth in Northern Zambia, the same cannot be considered for Cr and V; their source, though controversial, could be ascribed to the exotic input of mafic minerals during the exhumation stage and/or to their leaching from basement rocks. Our results confirmed the work of Mondillo et al. [19], and the analyzed FeO/OH from Kabwe only carry trace amounts of Ge (up to 11 ppm Ge), which are lower than those measured in other supergene ores, such as Cristal (see Section 5.1.3). According to Mondillo et al. [19], the lack of Ge in FeO/OH at Kabwe was likely related to their genesis in neutral to slightly basic conditions, not favorable for the Ge enrichment, and thus fits well with the absence of Ge in FeO/OH from the Kabwe 2, 3 and 4 clusters, and with the incorporation of most of the Ge in hydrothermal willemite preceding the supergene stage, which significantly decreased the Ge availability during the formation stage of FeO/OH.

6. Conclusions

Fe-oxy-hydroxides occurring in supergene non-sulfide deposits host a wide range of elements. These elements can be subdivided in two macro-groups: (i) elements that are ubiquitous in Zn non-sulfide ores, due to their concentration during the alteration process (i.e., Zn, Pb, Ca, Mn, Mg and Si), and (ii) elements (i.e., Cr, V, U, Y, Ge and Ga) that are concentrated in FeO/OH during their precipitation under very specific conditions, such as the nature of the primary ore or the exotic input of material, alteration history, etc. The statistical analysis of LA-ICP-MS data from FeO/OH occurring in four Zn non-sulfide deposits (i.e., Hakkari, Jabali, Cristal and Kabwe) has shown contrasting interelement associations, which reflect the diverse contribution of the intrinsic properties of the various ore systems, the prevailing ore-formation processes, as well as the environmental conditions, in defining the optimal conditions for metals up-taking in FeO/OH. Based on our data, the main findings are:

(A) FeO/OH occurring in non-sulfide ores evolving by direct replacement of sulfides and/or where pyrite is abundant in the primary ore (Cristal and Hakkari, respectively), and where a negligible buffering of the solutions led to an acidity-driven ore-formation process, are significantly enriched in Zn, Si, Pb, Ga and Ge.

(B) FeO/OH occurring in non-sulfide ores where the host carbonate rocks play a key role in buffering the solution (Jabali) are depleted in Zn, Pb, Si and Ge, and show relatively high contents in elements supplied to the system by the dissolution of dolomite (i.e., Mn).

(C) FeO/OH occurring in deposits where the input of exotic phases from the country rocks is significant may concentrate high amounts of unconventional metals (i.e., Cr and Co at Kabwe; Y at Cristal), depending on whether optimal pH-Eh conditions occur.

(D) FeO/OH occurring in the Kabwe ore body show a heterogeneous geochemical signature pointing to variable environmental conditions governing the ore formation process. Some FeO/OH show relatively high V and U concentrations, which indicate locally prevailing more basic conditions during the alteration process. Conversely, a few FeO/OH occurring in the intensively oxidized samples have high Zn and Si, commonly characteristic of an acid-driven formation process.

Supplementary Materials: The following are available online at http://www.mdpi.com/2075-163X/10/7/602/s1, Table S1: Mineral chemistry of goethites from the Zn-nonsulfides of Cristal and Kabwe. Major and minor elements were analyzed through EMPA (wt%), while trace elements were analyzed through LA-ICP-MS (ppm), Table S2: LA-ICP-MS of hematites from Zn-nonsulfides of Kabwe, Table S3: LA-ICP-MS Secondary standard values, Table S4: Mineral chemistry of goethites from the Zn-nonsulfides of Hakkari and Jabali. Major and minor elements were analyzed through EMPA (wt%), while trace elements were analyzed through LA-ICP-MS, Table S5: Summary of Principal Component Analysis, Figure S1: Boxplots showing the chemical composition of the studied FeO/OH from Kabwe [18]: (A) Goethite from Kabwe 1 (sample ID: MI10900), (B) and (C) Goethite and hematite from Kabwe 2, respectively (sample ID: BM1930-372), Figure S2: Boxplots showing the chemical composition of the studied FeO/OH from Kabwe [18]: (A) Goethite from Kabwe 3 (sample ID: OR5305), (B) Hematite from Kabwe 3 (sample ID: OR5305), (C) Goethite from Kabwe 3 (sample ID: BM.1985,MI29629 2/2), (D) Hematite from Kabwe 3 (sample ID: BM.1985,MI29629 2/2), Figure S3: Boxplots showing the chemical composition of the studied FeO/OH from Kabwe [18]: (A) Goethite from Kabwe 4 (sample ID: BM.1985,MI29631), (B) Hematite from Kabwe 4 (sample ID: BM.1985,MI29631), (C) Goethite from Kabwe 4 (sample ID: OR5309), (D) Hematite from Kabwe 4 (sample ID: OR5309).

Author Contributions: Conceptualization, L.S., M.B., F.P. and N.M.; software, L.S. and F.P.; validation, L.S., F.P. and N.M.; methodology and formal analysis, L.S. and N.M.; investigation, L.S., N.M. and M.B.; data curation, L.S., N.M. and F.P.; writing—original draft preparation, L.S. and F.P.; writing—review and editing, M.B. and N.M.; project administration, M.B.; funding acquisition, L.S., R.H. and N.M. All authors have read and agreed to the published version of the manuscript.

Funding: The research leading to these results has received funding from the European Union's Horizon 2020 research and innovation program, by a Marie Skłodowska-Curie Individual Fellowship (Project name GOSSAN, number 751103) awarded to R.H., supporting the fellowship of L.S. Additional funds are from the "Programma per il finanziamento della ricerca di Ateneo 2016–Progetto CEB", granted by Università degli Studi di Napoli Federico II (Italy) to N.M.

Acknowledgments: The authors are indebted to R. de' Gennaro and J. Spratt for the help and to Y. Buret respectively, during SEM and LA-ICP-MS analyses. Two anonymous reviewers are greatly thanked for their comments, which improved the original version of the manuscript.

Conflicts of Interest: The authors declare no conflict of interest.

References

1. Large, D. The geology of nonsulfide zinc deposits—An overview. *Erzmetall* **2001**, *54*, 264–274.
2. Hitzman, M.W.; Reynolds, N.A.; Sangster, D.F.; Allen, C.R.; Carman, C. Classification, genesis, and exploration guides for nonsulfide zinc deposits. *Econ. Geol.* **2003**, *98*, 685–714. [CrossRef]
3. Boni, M.; Mondillo, N. The "Calamines" and the "Others": The great family of supergene nonsulfide zinc ores. *Ore Geol. Rev.* **2015**, *67*, 208–233. [CrossRef]
4. Taylor, R. *Gossan and Leached Cappings, Field Assessment*; Springer: Berlin/Heidelberg, Germany, 2011.
5. Fendorf, S.; Eick, M.J.; Grossl, P.; Sparks, D.L. Arsenate and Chromate Retention Mechanisms on Goethite. 1. Surface Structure. *Environ. Sci. Technol.* **1997**, *31*, 315–320. [CrossRef]
6. Villalobos, M.; Leckie, J.O. Surface complexation modeling and FTIR study of carbonate adsorption to goethite. *J. Colloid. Interface Sci.* **2001**, *235*, 15–32. [CrossRef] [PubMed]
7. Antelo, J.; Avena, M.; Fiol, S.; Lopez, R.; Arce, F. Effects of pH and ionic strength on the adsorption of phosphate and arsenate at the goethite-water interface. *J. Colloid. Interface Sci.* **2005**, *285*, 476–486. [CrossRef] [PubMed]
8. Cornell, R.M.; Schwertmann, U. *The Iron Oxides: Structure, Properties, Reactions, Occurrences and Uses*; WILEY-VCH Verlag: Weinheim, Germany, 2003; p. 664.
9. Granados-Correa, F.; Corral-Capulin, N.G.; Olguin, M.T.; Acosta-Leon, C.E. Comparison of the Cd(II) adsorption processes between boehmite (gamma-AlOOH) and goethite (alpha-FeOOH). *Chem. Eng. J.* **2011**, *171*, 1027–1034.
10. Perelomov, L.V.; Pinskiy, D.L.; Violante, A. Effect of organic acids on the adsorption of copper, lead, and zinc by goethite. *Eurasian Soil Sci.* **2011**, *44*, 22–28. [CrossRef]
11. Mikulski, S.Z.; Oszczepalski, S.; Sadłowska, K.; Chmielewski, A.; Małek, R. Trace Element Distributions in the Zn-Pb (Mississippi Valley-Type) and Cu-Ag (Kupferschiefer) Sediment-Hosted Deposits in Poland. *Minerals* **2020**, *10*, 75. [CrossRef]

12. Blengini, G.A.; Nuss, P.; Dewulf, J.; Nita, V.; Peirò, L.T.; Vidal-Legaz, B.; Pellegrini, M. EU methodology for critical raw materials assessment: Policy needs and proposed solutions for incremental improvements. *Resour. Policy* **2017**, *53*, 12–19. [CrossRef]
13. Frenzel, M.; Kullik, J.; Reuter, M.A.; Gutzmer, J. Raw material 'criticality'—Sense or nonsense? *J. Phys. Appl. Phys.* **2017**, *50*, 123002. [CrossRef]
14. Bernstein, L.R. Geology and mineralogy of the Apex germanium-gallium mine, Washington County, Utah. *USGS* **1986**, *1577*, 1–9.
15. Bernstein, L.R.; Waychunas, G.A. Germanium crystal chemistry in hematite and goethite from the Apex Mine, Utah, and some new data on germanium in aqueous solution and in stottite. *Geochim. Cosmochim. Acta* **1987**, *51*, 623–630. [CrossRef]
16. Mondillo, N.; Boni, M.; Balassone, G.; Joachimski, M.; Mormone, A. The Jabali nonsulfide Zn–Pb–Ag deposit, western Yemen. *Ore Geol. Rev.* **2014**, *61*, 248–267. [CrossRef]
17. Mondillo, N.; Boni, M.; Balassone, G.; Villa, I.M. The Yanque prospect (Peru): From polymetallic Zn-Pb mineralization to a nonsulfide deposit. *Econ. Geol.* **2014**, *109*, 1735–1762. [CrossRef]
18. Mondillo, N.; Arfè, G.; Herrington, R.; Boni, M.; Wilkinson, C.; Mormone, A. Germanium enrichment in supergene settings: Evidence from the Cristal nonsulfide Zn prospect, Bongará district, northern Peru. *Miner. Depos.* **2018**, *53*, 155–169. [CrossRef]
19. Mondillo, N.; Herrington, R.; Boyce, A.J.; Wilkinson, C.; Santoro, L.; Rumsey, M. Critical elements in non-sulfide Zn deposits: A reanalysis of the Kabwe Zn-Pb ores (central Zambia). *Miner. Mag.* **2018**, *82* (Suppl. 1), S89–S114. [CrossRef]
20. Mondillo, N.; Accardo, M.; Boni, M.; Boyce, A.; Herrington, R.; Rumsey, M.; Wilkinson, C. New insights into the genesis of willemite (Zn_2SiO_4) from zinc nonsulfide deposits, through trace elements and oxygen isotope geochemistry. *Ore Geol. Rev.* **2020**, *118*, 103307. [CrossRef]
21. Santoro, L.; Boni, M.; Herrington, R.; Clegg, A. The Hakkari nonsulfide Zn-Pb deposit in the context of other nonsulfide Zn–Pb deposits in the Tethyan Metallogenic Belt of Turkey. *Ore Geol. Rev.* **2013**, *53*, 244–260. [CrossRef]
22. Santoro, L.; Boni, M.; Rollinson, G.K.; Mondillo, N.; Balassone, G.; Clegg, A.M. Mineralogical characterization of the Hakkari nonsulfide Zn(Pb) deposit (Turkey): The benefits of QEMSCAN®. *Miner. Eng.* **2014**, *69*, 29–39. [CrossRef]
23. Santoro, L.; Rollinson, G.K.; Boni, M.; Mondillo, N. Automated Scanning Electron Microscopy (QEMSCAN@) based mineral identification and quantification of the Jabali Zn-Pb-Ag Nonsulfide deposit (Yemen). *Econ. Geol.* **2015**, *110*, 1083–1099. [CrossRef]
24. Navarro-Ciurana, D.; Campos-Quispe, L.; Cardellach, E.; Catena, E.; Gómez-Gras, D.; Griera, A.; Corbella, M. Mineralogical and geochemical characterization of the Riópar non-sulfide Zn-(Fe-Pb) deposits (Prebetic Zone, SE Spain). *Ore Geol. Rev.* **2016**, *79*, 515–532. [CrossRef]
25. Arfè, G.; Mondillo, N.; Boni, M.; Balassone, G.; Joachimski, M.; Mormone, A.; Di Palma, T. The karst hosted Mina Grande nonsulfide zinc deposit, Bongará district (Amazonas region, Peru). *Econ. Geol.* **2017**, *112*, 1089–1110.
26. Arfè, G.; Mondillo, N.; Boni, M.; Joachimski, M.; Balassone, G.; Mormone, A.; Santoro, L.; Castro Medrano, E. The Rio Cristal Zinc prospect (Amazonas region, Northern Peru). Part II: An example of supergene zinc enrichments in tropical areas. *Ore Geol. Rev.* **2018**, *95*, 1076–1105.
27. Stavinga, D.; Jamieson, H.; Paradis, S.; Falck, H. Geochemical and Mineralogical Controls on Metal(loid) Mobility in the Oxide Zone of the Prairie Creek Deposit, NWT. *Geochem. Explor. Environ. A* **2017**, *17*, 21. [CrossRef]
28. Wood, S.A.; Samson, I.M. The aqueous geochemistry of gallium, germanium, indium and scandium. *Ore Geol. Rev.* **2006**, *28*, 57–102. [CrossRef]
29. Günay, Y.; Şenel, M. *Turkey Geological Map, 1:500,000 Scale, Cizre Sheet, No 18*; General Directorate of Mineral Research and Exploration: Ankara, Turkey, 2002.
30. Yigit, O. Mineral deposits of Turkey in relation to Tethyan metallogeny: Implications for future mineral exploration. *Econ. Geol.* **2009**, *104*, 19–51. [CrossRef]
31. Venter, M.; Robertson, M. *Desktop, Remote Sensing and Field Validation*; Internal Report; Red Crescent Resources A.Ş.: Ankara, Turkey, 2009.

32. Grodner, M. The Hakkari zinc oxide project, Turkey. In Proceedings of the IAEG–ZINC Conference, Cork, Ireland, 17–19 September 2010; pp. 23–26. Available online: http://www.iaeg.org/docs/2010/Zinc2010_Abstracts.pdf (accessed on 12 April 2020).
33. MSA Group Ltd. Technical Report on the Hakkari Zinc Project, NI 43–101, 3 August 2011. Available online: www.sedar.com (accessed on 12 March 2020).
34. Ceyhan, N. Lead isotope geochemistry of Pb-Zn deposits from Eastern Taurides, Turkey. Unpub. Master's Thesis, Graduate School of Natural and Applied Sciences of the Middle East Technical University, Ankara, Turkey, 2003; p. 105.
35. Reynolds, N.; Large, D. Tethyan zinc–lead metallogeny in Europe, North Africa, and Asia. *Econ. Geol. Spec. Publ.* **2010**, *15*, 339–365.
36. Hanilçi, N.; Öztürk, H.; Kasapci, C. Carbonate-Hosted Pb-Zn Deposits of Turkey. In *Mineral Resources of Turkey*; Springer: Cham, Switzerland, 2019; pp. 497–533.
37. Al Ganad, I.; Lagny, P.; Lescuyer, J.L.; Rambo, C.; Touray, J.C. Jabali, a Zn-Pb-(Ag) carbonate-hosted deposit associated with Late Jurassic rifting in Yemen. *Miner. Depos.* **1994**, *29*, 44–56. [CrossRef]
38. As-Saruri, M.A.; Sorkhabi, R.; Baraba, R. Sedimentary basins of Yemen: Their tectonic development and lithostratigraphic cover. *Arab. J. Geosci.* **2010**, *3*, 515–527. [CrossRef]
39. Roedder, E. Fluid inclusion evidence for the genesis of ores in sedimentary and volcanic rocks. In *Ores in Sediments, Sedimentary and Volcanic Rocks*; Wolf, K.H., Ed.; Elsevier: Amsterdam, The Netherlands, 1976; Volume 2, pp. 67–110.
40. Ostendorf, J.; Henjes-Kunst, F.; Mondillo, N.; Boni, M.; Schneider, J.; Gutzmer, J. Formation of Mississippi Valley–type deposits linked to hydrocarbon generation in extensional tectonic settings: Evidence from the Jabali Zn-Pb-(Ag) deposit (Yemen). *Geology* **2015**, *43*, 1055–1058.
41. Anglo Peruana. *A Re–evaluation of the Geology and Mineralization of the Charlotte Bongará Zinc Project, Amazonas, Northern Peru: Technical Report*; Anglo Peruana Terra S.A (former Consultora Minera Anglo Peruana S.A.): Lima, Peru, 2005.
42. Workman, A.W.; Reddick, J. *Technical Report on the Bongará Zinc Project, Yambrasbamba district, Amazonas Region, Northern Peru for Zinc One Resources Inc.* 2019 p. 184. Available online: https://zincone.com/site/assets/files/2341/bonara_zinc_mine_technical_report.pdf (accessed on 20 April 2020).
43. Mišković, A.; Spikings, R.A.; Chew, D.M.; Košler, J.; Ulianov, A.; Schaltegger, U. Tectonomagmatic evolution of Western Amazonia: Geochemical characterization and zircon U-Pb geochronologic constraints from the Peruvian Eastern Cordilleran granitoids. *Geol. Soc. Am. Bull.* **2009**, *121*, 1298–1324. [CrossRef]
44. Brophy, J.A. *Technical Report on the Rio Cristal Resources Corp. Bongará Zinc Project;* NI 43–101; 2012; p. 104. Available online: https://www.smv.gob.pe/ConsultasP8/temp/Amended_restated_TechnicalReport_NI43101.pdf (accessed on 20 April 2020).
45. Reid, C.J. Stratigraphy and Mineralization of the Bongara MVT Zinc-lead District, Northern Peru. Master's Thesis, University of Toronto, Toronto, ON, Canada, 2001; p. 179.
46. Basuki, N.I. Post-Early Cretaceous MVT Zn-Pb Mineralisation, Bongara Area, Northern Peru Fluid Characteristics and Constraints on Deposition Mechanisms. Unpublished Ph.D. Thesis, University of Toronto, Toronto, ON, Canada, 2006; p. 318.
47. Basuki, N.I.; Spooner, E.T.C. Fluid evolution and flow direction of MVT Zn-Pb related basinal brines, Bongará area, northern Peru: CL and fluid inclusion data [abs.]. In Proceedings of the Geological-Mineralogical Association of Canada-Society of Economic Geologists—Society for Geology Applied to Mineral Deposits Meeting, Quebec, QC, Canada, 26–28 May 2008; p. 13.
48. Basuki, N.I.; Spooner, E.T.C. Post-early Cretaceous Mississippi Valley Type Zn-Pb mineralization in the Bongará Area, Northern Peru: Fluid evolution and Paleo-Flow from fluid inclusions evidence. *Explor. Min. Geol.* **2009**, *18*, 25–39. [CrossRef]
49. Kamona, A.F.; Friedrich, G.H. Geology, mineralogy and stable isotope geochemistry of the Kabwe carbonate-hosted Pb–Zn deposit, Central Zambia. *Ore Geol. Rev.* **2007**, *30*, 217–243. [CrossRef]
50. Kampunzu, A.B.; Cailteux, J.L.H.; Kamona, A.F.; Intiomale, M.M.; Melcher, F. Sediment hosted Zn-Pb-Cu deposits in the Central African Copperbelt. *Ore Geol. Rev.* **2009**, *35*, 263–297. [CrossRef]
51. Moore, T.A. *The Geology of the Chisamba Area: Explanation of Degree Sheet 1428, SW Quarter*; Lusaka Govt. Priner: Lusaka, Zambia, 1964.

52. Cairney, T.; Kerr, C.D. The geology of the Kabwe area: Explanation of degree sheet 1428, NW quarter. *Geol. Surv. Zambia Rep.* **1998**, *47*, 40.
53. Kamona, A.F. The Carbonate-Hosted Kabwe Pb– Zn Deposit, Central Zambia. Ph.D. Thesis, Technical University of Aachen, Aachen, Germany, 1993.
54. Terracciano, R. Willemite Mineralisation in Namibia and Zambia. Ph.D. Thesis, Università degli Studi di Napoli Federico II, Napoli, Italy, 2008; p. 178.
55. Leach, D.L.; Sangster, D.; Kelley, K.; Large, R.; Garven, G.; Allen, C.; Gutzmer, J.; Walters, S. Sediment-hosted lead-zinc deposits: A global perspective. *Econ. Geol.* **2005**, *100*, 561–607.
56. Heijlen, W.; Banks, D.A.; Muchez, P.; Stensgard, B.M.; Yardley, B.W.D. The nature of mineralizing fluids of the Kipushi Zn-Cu deposit, Katanga, Democratic Republic of Congo: Quantitative fluid inclusion analysis using Laser Ablation ICP-MS and bulk Crush-Leach methods. *Econ. Geol.* **2008**, *103*, 1459–1482. [CrossRef]
57. De Putter, T.; Ruffet, G. Supergene manganese ore records 75 Myr-long Campanian to Pleistocene geodynamic evolution and weathering history of the Central African Great Lakes Region—Tectonics drives, climate assists. *Gondwana Res.* **2020**, *83*, 96–117. [CrossRef]
58. Zachariáš, J.; Wilkinson, J. ExLAM 2000: Excel VBA application for processing of transient signal from laser ablation (LA-ICPMS) of fluid inclusions and solid phases. In Proceedings of the ECROFI-XIX Biennial Conference on European Current Research on Fluid Inclusions, Bern, Switzerland, 17–20 July 2007.
59. Reimann, C.; Filzmoser, P.; Garrett, R.; Dutter, R. *Statistical Data Analysis Explained: Applied Environmental Statistics with R*; John Wiley & Sons: Hoboken, NJ, USA, 2011.
60. Martín-Fernández, J.A.; Barceló-Vidal, C.; Pawlowsky-Glahn, V. Dealing with zeros and missing values in compositional data sets using nonparametric imputation. *Math. Geol.* **2003**, *35*, 253–278. [CrossRef]
61. Whitney, D.L.; Evans, B.W. Abbreviations for names of rock-forming minerals. *Am. Miner.* **2010**, *95*, 185–187. [CrossRef]
62. Davidson, L.E.; Shaw, S.; Benning, L. The kinetics and mechanisms of schwertmannite transformation to goethite and hematite under alkaline conditions. *Am. Mineral.* **2008**, *93*, 1326–1337. [CrossRef]
63. Vu, H.P.; Shaw, S.; Brinza, L.; Benning, L.G. Crystallization of hematite (alpha-Fe(2)O(3)) under alkaline condition: The effects of Pb. *Cryst. Growth Des.* **2010**, *10*, 1544–1551. [CrossRef]
64. Vu, H.P.; Shaw, S.; Brinza, L.; Benning, L.G. Partitioning of Pb(II) during goethite and hematite crystallization: Implications for Pb transport in natural systems. *Appl. Geochem.* **2013**, *39*, 119–128. [CrossRef]
65. Schwertmann, U.; Murad, E. Effect of pH on the formation of goethite and hematite from ferrihydrite. *Clays Clay Min.* **1983**, *31*, 277–284. [CrossRef]
66. Schwertmann, U.; Friedl, J.; Stanjek, H. From Fe (III) ions to ferrihydrite and then to hematite. *J. Colloid. Interface Sci.* **1999**, *209*, 215–223. [CrossRef]
67. Schwertmann, U.; Cornell, R.M. *Iron Oxides in the Laboratory*, 2nd ed.; Wiley-VCH Verlag: Weinheim, Germany, 2000; p. 188.
68. Schwertmann, U.; Stanjek, H.; Becher, H. Long-term in vitro transformation of 2-line ferrihydrite to goethite/hematite at 4, 10, 15 and 25 °C. *Clay Min.* **2004**, *39*, 433–438. [CrossRef]
69. Frenzel, M.; Hirsch, T.; Gutzmer, J. Gallium, germanium, indium, and other trace and minor elements in sphalerite as a function of deposit type—A meta-analysis. *Ore Geol. Rev.* **2016**, *76*, 52–78. [CrossRef]
70. Hieronymus, B.; Kotschoubey, B.; Boulègue, J. Gallium behaviour in some contrasting lateritic profiles from Cameroon and Brazil. *J. Geochem. Explor.* **2001**, *72*, 147–163. [CrossRef]
71. Lu, P.; Nuhfer, N.; Kelly, S.; Li, Q.; Konishi, H.; Elswick, E.; Zhu, C. Lead coprecipitation with iron oxyhydroxide nano-particles. *Geochim. Cosmochim. Acta.* **2011**, *75*, 4547–4561. [CrossRef]
72. Swedlund, P.; Webster, J.; Miskelly, G. Goethite adsorption of Cu(II), Pb(II), Cd(II), and Zn(II) in the presence of sulfate: Properties of the ternary complex. *Geochim. Cosmochim. Acta* **2009**, *73*, 1548–1562. [CrossRef]
73. Dash, B.; Rath, S.S. A thorough understanding of the adsorption of Ni (II), Cd (II) and Zn (II) on goethite using experiments and molecular dynamics simulation. *Sep. Purif. Technol.* **2020**, *240*, 116649. [CrossRef]
74. Boni, M. Non-sulfide zinc deposits: A new-(old) type of economic mineralization. *SGA News* **2003**, *15*, 6–11.
75. McPhail, D.C.; Summerhayes, E.; Jayaratne, V.; Christy, A. Hemimorphite solubility and stability of low-T zinc minerals. *Geochim. Cosmochim. Acta* **2006**, *70*, 36. [CrossRef]
76. Warren, J. Dolomite: Occurrence, evolution and economically important associations. *Earth Sci. Rev.* **2000**, *52*, 1–81. [CrossRef]

77. Dublet, G.; Juillot, F.; Brest, J.; Noël, V.; Fritsch, E.; Proux, O.; Morin, G. Vertical changes of the Co and Mn speciation along a lateritic regolith developed on peridotites (New Caledonia). *Geochim. Cosmochim. Acta* **2017**, *217*, 1–15. [CrossRef]
78. Liu, H.; Pourret, O.; Guo, H.; Bonhoure, J. Rare earth elements sorption to iron oxyhydroxide: Model development and application to groundwater. *Appl. Geochem.* **2017**, *87*, 158–166. [CrossRef]
79. Boni, M.; Terracciano, R.; Evans, N.J.; Laukamp, C.; Schneider, J.; Bechstaädt, T. Genesis of vanadium ores in the Otavi Mountainland, Namibia. *Econ. Geol.* **2007**, *102*, 441–469. [CrossRef]
80. Peacock, C.L.; Sherman, D.M. Vanadium (V) adsorption onto goethite (α-FeOOH) at pH 1.5 to 12: A surface complexation model based on ab initio molecular geometries and EXAFS spectroscopy. *Geochim. Cosmochim. Acta* **2004**, *68*, 1723–1733. [CrossRef]
81. Sherman, D.M.; Peacock, C.L.; Hubbard, C.G. Surface complexation of U (VI) on goethite (α-FeOOH). *Geochim. Cosmochim. Acta* **2008**, *72*, 298–310. [CrossRef]
82. Carlisle, D. Concentration of uranium and vanadium in calcretes and gypcretes. *Geol. Soc. Lond. Spec. Publ.* **1983**, *11*, 185–195. [CrossRef]
83. Freyssinet, P.; Butt, C.R.M.; Morris, R.C.; Piantone, P. Ore-forming processes related to lateritic weathering. *Econ. Geol.* **2005**, *100*, 681–722.